ISCI, Volume *22*

Supplemental Information

All-Optical Volumetric Physiology

for Connectomics in Dense Neuronal Structures

Chiao Huang, Chu-Yi Tai, Kai-Ping Yang, Wei-Kun Chang, Kuo-Jen Hsu, Ching-Chun Hsiao, Shun-Chi Wu, Yen-Yin Lin, Ann-Shyn Chiang, and Shi-Wei Chu

Supplemental Figures

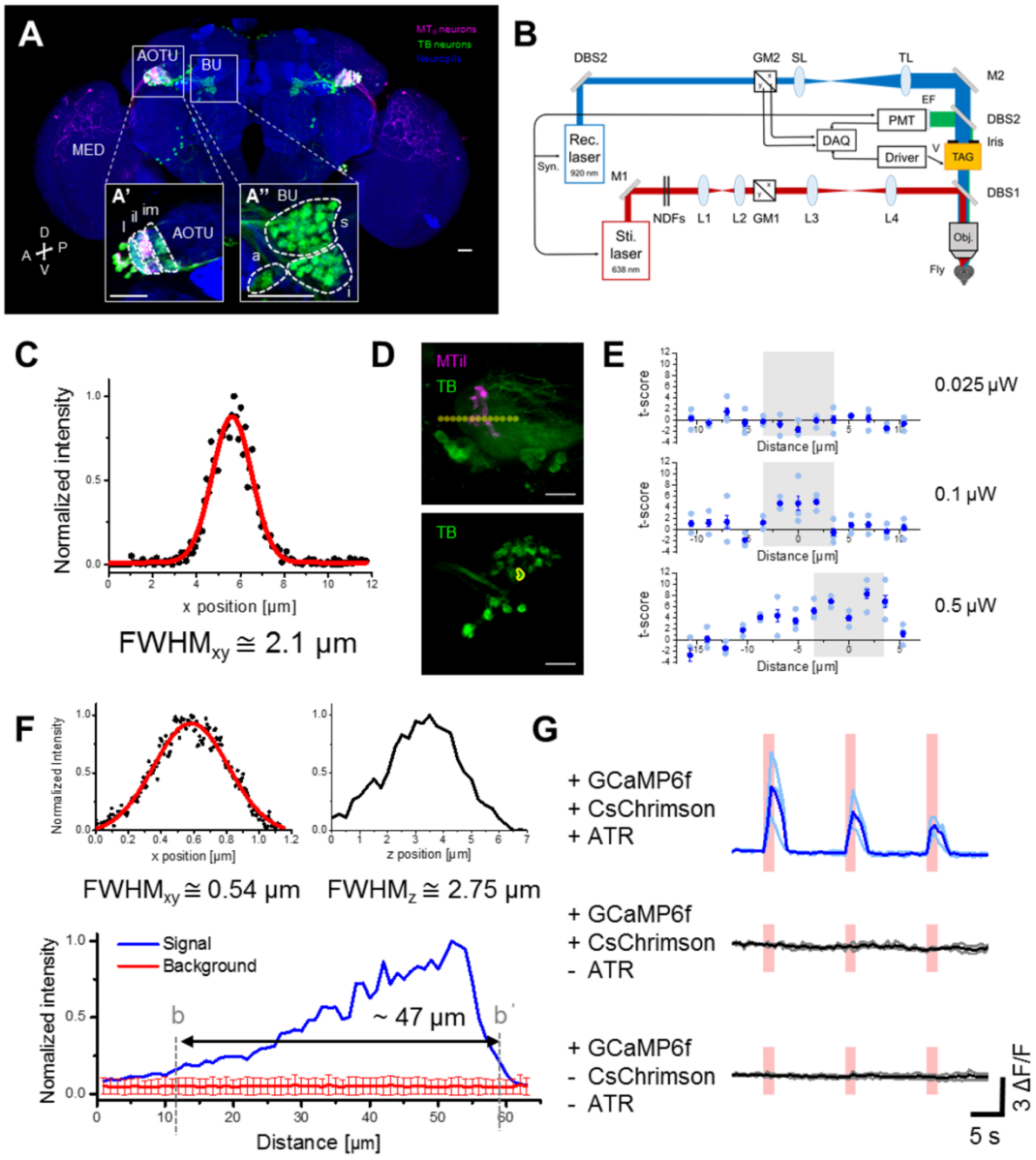

Figure S1. *Drosophila* anterior visual pathway (AVP) and specification of all-optical physiology (AOP) platform. (Related to Figures 1-2)

(A-A'') *Drosophila* AVP with MT_{il} neurons (connecting the medulla [MED] and the intermediate-lateral anterior optical tubercle [AOTUil]) and TB neurons (connecting the AOTU and the bulb [BU]). MT_{il} neurons (magenta) and TB neurons (green) are shown with neuropils marker (blue). The substructure of AOTU and BU are given in insets (A') and (A''), respectively, representing the sub-compartments of the AOTU (intermediate medial AOTU [AOTUim], intermediate lateral AOTU [AOTUil], lateral AOTU [AOTUl]) and the BU (superior BU [BUs], inferior BU [BUi],

and anterior BU [BUa]). In the following all-optical physiology demonstrations, the axon terminal of MT_{il} neurons (AOTUil) are stimulated, and (volumetric) recordings are taken from the axon terminal of TB neurons (BU). Abbreviations of coordinates: A, anterior; P, posterior; V, ventral; D, dorsal; L, lateral; M, medial. Scale bar: 20 μm.

(B) System setups of single-photon stimulation and two-photon imaging in all-optical physiology platform. Sti. laser, stimulation laser; Rec. laser, recording laser; M, mirror; NDF, ND filter; L, lens; GM, galvo mirrors; DBS, dichroic beam splitters; SL, scan lens; TL, tube lens; TAG, tunable acoustic gradient-index lens; Obj., objectives; EF, emission filter; PMT, photomultiplier tubes; DAQ, data acquisition device; Syn. Synchronization system. All-optical physiology with single-depth recording is achieved with the TAG turned off while fast volumetric imaging is achieved with the TAG turned on.

(C) Lateral point-spread-function of stimulation laser. Black dots represent the signal, and the red line represents Gaussian fitting with lateral full-width-of-maximum (FWHMxy) ≅ 2.1 μm. Confinement of stimulation is verified by all-optical physiology on CsChrimson.mVenus-expressing MT_{il} neurons and GCaMP6f-expressing TB neurons in (D-E).

(D) Top: MT_{il} neurons (magenta color) and TB neurons (green color) in the AOTU. Sequential stimulation is applied to sites indicated by yellow circles with three different power. Bottom: TB neurons (green color) in BU microglomeruli. Response of a single microglomerulus (in the yellow circle) to various stimulation powers is shown in (E). Scale bar: 10 μm.

(E) The response of a single microglomerulus with various stimulation power. Stimulation at each site is repeated three times and each response is presented as a t-score based on the analysis of a GLM (generalized linear model, see Methods). The responses were shown in plots in the right panel and the corresponding power of the stimulation laser are shown on the right side of the panel. Light blue dots in the plots are the response to each repeated stimulation, and their averages are presented as dark blue dots (mean ± SEM). The gray rectangle indicates the region where MT_{il} neurons are localized. The results show that with the proper control of stimulation power, TB neurons had detectable Ca^{2+} activity only when stimulation was posed in the range where MTil neurons were localized.

(F) Top: Lateral/axial (left/right) point spread functions of recording laser with the signal shown in black and the Gaussian fitting shown in red. The results fit well with the theoretical prediction (FWHMxy, theo = 0.54 μm, FWHMz, theo = 2.75 μm) with effective NA = 0.8. Down: The axial recording range of the tunable acoustic gradient-index (TAG) lens. The blue curve shows the signal intensity from a fluorescent sphere, and the red curve shows the background intensity (mean ± SD). The range marked by the dashed line b and b' in the position where the signal is deviated from the mean of background by 2 SD.

(G) AOP on three groups of flies to verify the effectiveness of optogenetic stimulation and recording, and the prevention of sensory-evoked Ca^{2+} response. Top: Flies with the TB neurons expressing GCaMP6f, the MT_{il} neurons expressing CsChrimson, and with all-trans retinal (ATR) feeding. Middle: Flies with TB neurons expressing GCaMP6f, MT_{il} neurons expressing CsChrimson, but without ATR feeding. Bottom: Flies with only the TB neurons expressing

GCaMP6f and without ATR feeding. The red bars indicate laser stimulation durations with ~ 0.8 μW power (n = 3 flies in each groups). Responses of individual flies are presented as light blue/gray curves and averaged responses are presented as blue/black curves. Detectable Ca^{2+} activity only appeared in the fruit flies expressing GCaMP6f and CsChrimson with feeding ATR (Top), indicating the validity of the AOP system, and confirmation that the sensory-evoked response is avoided.

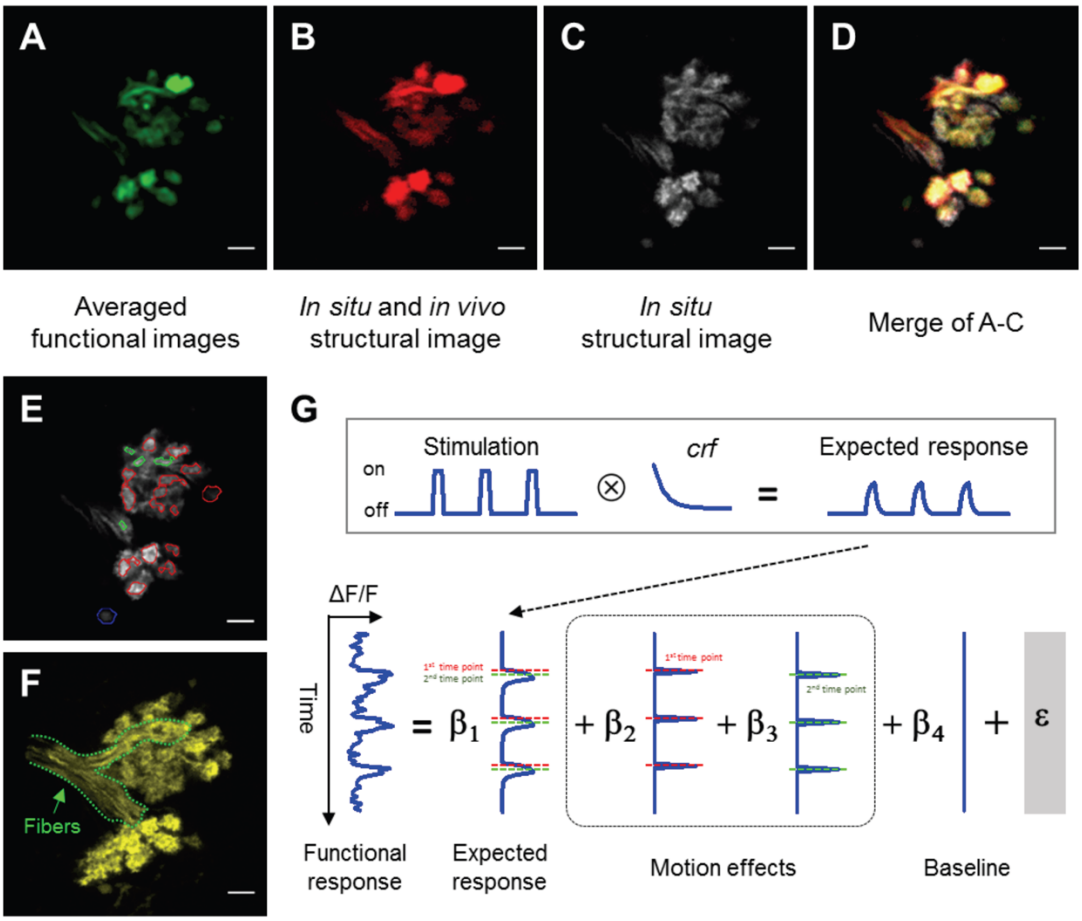

Figure S2. Analysis of structural and functional images (Related to Figures 1-3)

(A-D) Registration of low-speed scanning images and functional images: (A) Averaged image from high-speed time-lapse functional images. (B) Low speed *in situ* and *in vivo* structural image. (C) Low speed *in vivo* image of fixed brain acquired with higher laser power and lower imaging speed. (D) Merged image of (A)-(C). Scale bar: 5 μm.

(E) Microglomeruli extraction from (C). The extracted regions (shown with circles) are sub-classified into three types: BU microglomeruli (red circles), neuron fibers (green circles, see (F)), and non-BU structures (blue circle, only visible in (C), but not in (A) and (B)). Both green and blue circles are excluded from analysis. Scale bar: 5 μm.

(F) Maximum-intensity projection of neuronal 3D structure with fibers marked with dotted lines. Scale bar: 5 μm.

(G) Functional response analysis using generalized linear models (GLM). Detailed descriptions can be found in the Methods section.

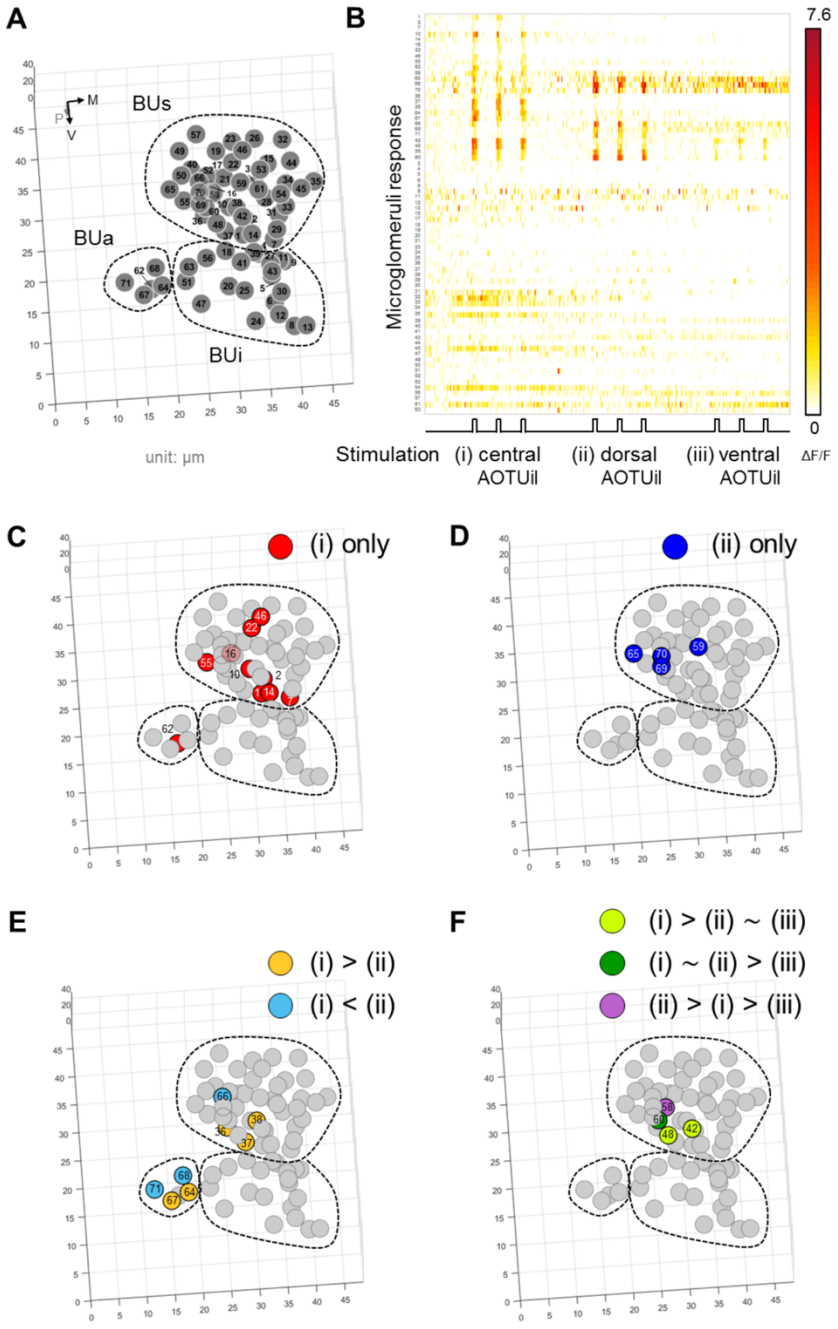

Figure S3. Volumetric recording of microglomeruli in the bulb (BU) (Related to Figures 2-3)

(A) The 3D position of microglomeruli in the BU extracted from Figure 2B and labeled with numbers to show individual responses in Figure 2C and S3B.

(B-F) Functional response of BU microglomeruli while stimulating the (i) central, (ii) dorsal, and (iii) ventral intermediate lateral AOTU (AOTUil), corresponding to the positions marked in Figure 3B. (B) Functional response of all microglomeruli with ΔF/F shown in color codes. The responses are grouped and sorted according to their responses to the three sites of stimulation (i.e., activation

stimulations determined by GLM and relative response strength profile among the three sites of stimulation).

(C-F) Grouping of these microglomeruli in a sorted sequence with spatial information. (C) and (D) The 3D distribution of microglomeruli that had detectable Ca^{2+} activity following by the stimulation of (i) and (ii), respectively. (E) Microglomeruli have detectable Ca^{2+} activity following stimulation of (i) and (ii). This group is further divided into two sub-groups (i.e., response strength (i) > (ii) [brown color], and response strength (i) < (ii) [cyan color]) (F) Microglomeruli have detectable Ca^{2+} activity following by the stimulation of all three sites. There are three different response strengths: 1) response strength (i) > (ii) ~ (iii) (light green color), 2) response strength (i) ~ (ii) > (iii) (green color), and 3) response strength (ii) > (i) > (iii) (purple color).

Transparent Methods

Fly strains

Fly strains were reared on a cornmeal-yeast-agar medium at 25 °C and 70% relative humidity following a 12/12-hr light/dark cycle. MTil neurons were labeled with LexAop-CsChrimson.mVenus (in attP18) in GR52532-LexA. TB neurons were labeled with UAS-GCaMP6f in VT50183-GAL4. The GR52532-LexA, LexAop-CsChrimson.mVenus, and UAS-GCaMP6f were ordered from the Bloomington Drosophila Stock Center (BDRC). The VT50183-GAL4 was ordered from the Vienna Drosophila Resource Center (VDRC).

Immunolabeling and confocal imaging

The *ex-vivo* images of AVP (Figure S1A) were acquired using confocal laser-scanning microscopy. Brains of adult flies expressing GCaMP6f and CsChrimson.mVenus were dissected in cold isotonic phosphate-buffered saline (PBS) and fixed in PBS containing 4% paraformaldehyde for 30 minutes. Brains were placed in PBS containing 2% Triton X-100 and 10% normal goat serum (NGS) before being degassed in a vacuum for 1 hr to remove air from the tracheal system; the solution was left in the same solution at 4 °C overnight to block non-specific labeling and increase antibody penetration. Immunohistochemistry was sequentially performed in PBS containing 1% NGS, Triton X-100, and following antibodies. The primary antibody was used mouse 4F3 anti-Discs large (1:50, Developmental Studies Hybridoma Bank (DSHB), University of Iowa) at 4 °C for two days. After two days, the tissue was washed and then incubated with biotinylated goat anti-mouse IgG secondary antibody (1:250, B2763, Molecular Probes) at 25°C for one day. Next, the tissue was washed and then incubated Alexa Fluor 635-conjugated streptavidin (1:500, S32364, Invitrogen) at room temperature for 24 hours for detection. Finally, after three 20 min washes, the immunolabeled samples were transferred to *FocusClear*™ (CelExplorer, Taiwan) for clearing and mounting before imaging. Immunolabeled adult brains

were imaged using a Zeiss LSM710 confocal microscope with 40x/NA 1.2 water-immersion objective (421767-9971-711, ZEISS, Germany). Signals of GCaMP6f, mVenus, and Alexa Fluor 635 were acquired using the combination of excitation wavelength, λ_{ex}, and detection wavelength, λ_{det}, at a range of λ_{ex} = 488 nm, λ_{det} = 500 ~ 550 nm, λ_{ex} = 514 nm, λ_{det} = 525 ~ 561 nm, and λ_{ex} = 633 nm, λ_{det} = 650 ~ 700 nm, respectively.

System setup of all-optical physiology platform

The system setup, which was composed of stimulation and recording arms, is shown in Figure S1B. In the stimulation arm, a 638 nm diode laser (iBeam smart, TOPTICA Photonics AG, Germany), whose incident power was controlled by two neural density filters (ND10B and ND20B, Thorlabs, NJ), was used as the light source. A telescope formed by two convex lenses (AC254-040-A-ML, Thorlabs, NJ) was placed in front of the galvo-mirrors to enable axial shift of the focal plane of the stimulation spot. A pair of galvo-mirrors (6200H, Cambridge Technology, MA) and a collimator with two convex lenses (LA1708-A-ML and AC254-200-A-ML, Thorlabs, NJ) were used to control the lateral position of the stimulation spot at the focal plane of a 40x/NA 1.0 water-immersion objective (421462-9900-000, Zeiss, Germany). The recording beam, with detailed description in the following, were also focused by this objective. In the recording arm, a commercial two-photon laser scanning microscope (LSM 780, Zeiss, Germany) that was equipped with a Ti:sapphire laser and non-descanned photomultiplier tubes (PMT) were used as the mainframe. The Ti:sapphire laser was tuned at 920 nm for optimal GCaMP6f excitation. A TAG lens (TAG 2.0, TAG Optics Inc., NJ) with 400-875 nm and 915-1350 nm wavelength ranges was inserted in the recording path directly on top of the objective to achieve extension of the axial recording range. The position prevented defocusing of the emission to reach maximum collection efficiency, similar to the de-scan process (Hsu et al., 2017). During volumetric recording, the TAG lens worked with a 144 kHz driving frequency (leading to 5.5 mm-size effective aperture) and 1

m^{-1} optical power. No significant aberration was found throughout axial recording range (Hsu et al., 2017). A notch dichroic beam splitter (NFD01-633-25x36, Semrock, NY) was placed between the TAG lens and the objective to reflect the stimulation laser onto the objective without being affected by the TAG lens. A home-made mount was used to integrate the TAG lens, beam splitter, and objective. The point spread functions of the stimulation laser were determined by glass reflection, and the point-spread function/axial recording range of the recording laser were determined by 200 nm- and 1 μm-size fluorescent microspheres (TetraSpeck™ Fluorescent Microspheres Size Kit, ThemoFisher, MA), individually.

A home-built LabVIEW program was used to synchronize the galvo-mirrors and the onset of the stimulation laser with a 250 kS/s data acquisition system (PCIe6321, National Instrument, TX). A 10 MS/s data acquisition system (PCIe8361, National Instrument, TX) was used to acquire volumetric images by recording the pixel/line trigger signals of LSM 780, the TAG trigger signal, and the PMT output. With the TAG lens resonant at 144 kHz, the 10 MHz sampling rate acquired 70 data points in one period, and each depth was sampled twice. By averaging the doubly sampled signals, our system provided 35 axial layers in a volumetric image. The volumetric images were reconstructed using a home-made MATLAB (R2107a, MathWorks) program. Since the TAG lens scanned the focus in the z-direction in a sinusoidal pattern, volumetric images were reconstructed by taking these patterns into account. More details can be found in our recent work (Hsu et al., 2019).

Due to the high scanning speed of the TAG lens, the volume rate was based on the lateral scanning pixel (pix.) number. In the current study, a ~ 9 Hz volume rate was expected with a 7 μs pixel duration (equal to the resonance period of the TAG lens) with 128(x)×128(y) sampling pixels. However, our volume rate was limited by the pixel dwell duration and x-y raster scanning scheme

of the commercial microscope (LSM 780, ZEISS). For pixel dwell duration, no arbitrary choice was allowed. In principle, it is best to choose the pixel dwell time that equals or slightly exceeds the 7 μs resonance period of the TAG lens. Nevertheless, the minimum allowable pixel dwell duration was 12.6 μs. In terms of the raster scanning scheme, it takes ~ 550 μs (equal to 44 pixel dwell durations) for the scanner to switch between each line during the scanning process; therefore, when the field of view (FOV) is set as 256(x)×128(y) pixels, the time it takes to scan is equivalent to the time it takes to scan across 300(x)×128(y) pixels. In addition, when we set the FOV with fewer scanned pixels (e.g., 128(x)×128(y)), the imaging speed, interestingly, was even slower than that of 256(x)×128(y) pixels. This was possibly due to the mechanical design of the LSM 780. Therefore, to achieve a higher imaging speed, we chose to use the 256(x)×128(y) setting even though we only used half of it to cover a square region of the BU structure. The reasons above all led to the reduction in volume speed. Specifically, the volume acquisition time was 300(x)×128(y)×12.6 μs (pixel dwell time) ≅ 484 ms, which led to a volume rate of 2 Hz. Although this speed was still enough to capture the calcium response and identify activated microglomeruli, further enhancement is necessary to realize higher volumetric imaging speed.

All-optical physiological measurement

After 5 days of all-trans-retinal feeding, the fruit fly was anaesthetized on ice and singly mounted in a holder before the AOP experiments. The cuticle above the brain was removed, and the brain was immersed in adult-hemolymph like (AHL) saline (108 mM NaCl, 5 mM KCl, 2 mM $CaCl_2$, 8.2 mM $MgCl_2$, 4 mM $NaHCO_3$, 1 mM NaH_2PO_4, 5 mM trehalose, 10 mM sucrose and 5 mM HEPES; pH 7.5, 265 mOsm, (Wang et al., 2007)) before fixation in agarose on a steel plane with the anterior side facing the objective. Although the stimulation site, AOTUil (where MT_{il} neuronal axons terminate, expressing CsChrimson.mVenus), and recording site, BU (where TB neuronal axons terminate, expressing GCaMP6f), in AOP measurements should be

distinguished by different excitation lasers (i.e., λ_{ex} = 514 nm, λ_{det} = 520 ~ 560 nm for mVenus and λ_{ex} = 920 nm, λ_{det} = 500 ~ 550 nm for GCaMP6f), the flies did not respond to optogenetic stimulation after imaging with a 514 nm laser. This is due to the spurious activation of CsChrimson because 514 nm is within its activation spectrum. Therefore, both AOTUil and BU were recognized using 920 nm laser-excitation imaging with a 500~550 nm detection spectrum. AOTUil was identified by the higher detection signal elicited by mVenus and GCaMP6f due to the structural overlapping of MT_{il} and TB neurons. After determining the stimulation and recording sites, we began recording with the Ti:sapphire laser. After the recording started, the first stimulation was delayed for a 10-20-s period to avoid transient artifacts resulting from the initialization of the recording laser. After this brief period, the stimulation was applied over 10 s with a 20% duty cycle (2 s on, 8 s off), repeated three times. The power of the 638 nm stimulation laser after the objective was < 0.8 μW for both the single-section and volumetric recordings, and the powers of the 920 nm recording laser after objective were < 2.8 mW and < 8.2 mW in the single-section and volumetric recording, respectively. We did not observe apparent heat damage or photobleaching during repeated stimulation and recording on the same *Drosophila* brain during either the single-section or volumetric recordings. After AOP measurements, *in vivo* structural imaging of MT_{il} and TB neurons (Figure 3B) was performed by excitation wavelength, λ_{ex}, and detection wavelength, λ_{det}, range of λ_{ex} = 920 nm, λ_{det} = 500 ~ 550 nm and λ_{ex} = 514 nm, λ_{det} = 520 ~ 560 nm, respectively.

Structural image acquisition and registration with functional imaging

To precisely determine the location of each microglomerulus, the structure of the BU was visualized by low-speed scanning after functional imaging. We used two steps for structural image acquisition and registration. First, *in situ* and *in vivo* 3D structural images of the BU were acquired by low-speed two-photon microscopy, and the z-stack was obtained via slow objective translation. During this initial acquisition, the *Drosophila* was still alive; therefore, the fluorescence intensity

profile was similar to that of functional imaging. Second, the flies were fixed in 4% paraformaldehyde in PBS for 30 minutes, and *in situ* high-contrast structural images of the fixed brain were acquired with higher laser power (~ 20 mW). The *in-situ* images were used as the reference images in order to identify BU microglomeruli.

To register structural and functional images (see Fig. S2), all time-lapsed functional images of one brain were first aligned (Guizar-Sicairos et al., 2008) and averaged to avoid motion artifacts and improve contrast (Figure S2A). Then, the averaged images were matched with *in situ* and *in vivo* structural images (Figure S2B), which have similar fluorescent intensity profiles, by finding the maximum cross correlation. Then, the matched images were used to register the second *in situ* high-contrast images (Figure S2C-D) by finding the maximum cross-correlation, and the *in-situ* images were used to aid microglomeruli extraction.

Microglomeruli extraction

Individual microglomeruli were extracted from the structural image based on a home-built MATLAB program for gray value morphological analysis, and the extraction was performed according to the following steps:

1. Gray-scale opening and closing (Vincent, 1993) were performed to remove the noise of the images.

2. Due to non-uniform intensity of each microglomerulus, regional maxima were identified as preliminarily detected regions of microglomeruli through H-maxima transform (Soille, 2013).

3. To further improve the segmentation of densely distributed microglomeruli, boundaries were formed for different microglomeruli using the watershed transformation (Meyer, 1994). After these processes were completed, we only retained the extracted regions with sufficient signal intensity and a proper area (2–4 μm in diameter). The regions with extremely low intensity or too small of an area could generate an out-of-focus signal, so we excluded these regions from the follow-up

analysis. Individual microglomeruli were marked by thresholding the gray value in each extracted region (Figure S2E).

The microglomeruli were extracted depth-by-depth for volumetric imaging. If an extracted microglomerulus only existed in one axial layer, it was also excluded from analysis since the digital axial resolution of our platform is better than the optical axial resolution. In addition, because the extraction process was based on fluorescence intensity, other neuronal structures, such as fibers, may have also been extracted. Based on their location and morphology, we excluded these regions in order to prevent confusion during functional analysis (Figure S2E-F).

Generalized linear model (GLM) analysis

The functional responses in AOP were analyzed using a generalized linear model (GLM) (Lütcke et al., 2013; Miri et al., 2011). In order to avoid translational motion artifacts, each time-lapsed functional image was first aligned in space (Guizar-Sicairos et al., 2008). With the assumption that single microglomeruli serve as functional units, fluorescent signals of multiple pixels in a single microglomerulus were averaged as one functional response for analysis. Temporal ΔF/F of each microglomerulus response was then calculated by $\Delta F/F = (F - F_{mean})/F_{mean}$, where F is the signal at each frame, and F_{mean} is the mean signal of the first 10 frames before stimulation. To identify activated microglomeruli, the temporal ΔF/F of each microglomerulus was analyzed using a GLM based on known stimulation on/off time and duty cycle. The model is defined by the following equation:

$$y = X\beta + \varepsilon$$

where $y_{n\times1}$ is the data column vector corresponding to the temporal ΔF/F of the response in a single microglomeruli with n sampling frames, $X_{n\times4}$ is a predictor matrix with four predictors in each column ($X_{n\times4}$= [X_1 X_2 X_3 X_4]), $\beta_{4\times1}$ is the weight column vector of predictors, and $\varepsilon_{n\times1}$ is

the error column vector. As shown in Figure S2G, we used four predictors in $X_{n\times4}$, including the expected response (X_1), motion effect in the first two individual frames in each stimulation (X_2 and X_3), and baseline (X_4).

The expected response predictor, X_1, is defined by the convolution of a rectangular function which represents stimulation on/off duration and the calcium response function (crf) which is defined as follows (Seelig and Jayaraman, 2013): $crf \sim \left(1 - e^{-\frac{t-t_0}{\Gamma_{on}}}\right)\left(e^{-\frac{t-t_0}{\Gamma_{off}}}\right) \approx \left(e^{-\frac{t-t_0}{\Gamma_{off}}}\right)$ where the t is imaging time point, based on multiples of 500 ms acquisition time, t_0 is the onset time of stimulation, and Γ_{on} and Γ_{off} are rise and decay time constants of the calcium indicator, respectively. Since Γ_{on} of GCaMP6f is in the order of tens of milliseconds (~ 80 ms, (Chen et al., 2013)) and much smaller than $t - t_0$, the term $\left(1 - e^{-\frac{t-t_0}{\Gamma_{on}}}\right)$ in crf is neglected. The off constants, Γ_{off}, in living *Drosophila* are determine by fitting ΔF/F of the experimental results as 588.8 $\pm$ 71.0 ms (n = 7 responses from 3 flies), which is close to the reported results seen in dissociated neuronal cultures (Chen et al., 2013).

The motion effect predictors (X_2 and X_3) play roles in differentiating and excluding jitter events from real activations (see Figure S2G). In the current experiment, we observed that *Drosophila* sometimes jittered at the beginning of each stimulation and caused the ΔF/F to change. Since neurons are not rigid and jitter only happened in small parts of neurons rather than whole structure, this motion artifact was difficult to compensate for through spatial image alignment. Therefore, in addition to the expected response predictor, we set one motion effect predictor (X_2) at the beginning of stimulation. However, motion effects may last 0.5-1 s after stimulation. Since the volume rate was about 2 Hz, it was necessary to add a second motion effect predictor (X_3).

With the predictors mentioned above, the weight for each predictor in $\beta_{4\times1}$ was acquired

($\beta_{4\times1} = [\beta_1\ \beta_2\ \beta_3\ \beta_4]^{\mathrm{T}}$) using the minimum least squared error method (minimum $\varepsilon^{\mathrm{T}}\varepsilon$). The activated response was identified using a two-tailed t-test and rejecting H_0: $\beta_1 = 0$ ($P < 0.001$ significance level). The t-scores were calculated using the following equation:

$$\text{t-score} = \frac{c^{\mathrm{T}}\beta}{\sqrt{Var(\varepsilon)c^{\mathrm{T}}(X^{\mathrm{T}}X)^{-1}c}}$$

where the contrast vector $c = [1\ 0\ 0\ 0]$.